Electronic and vibrational predissociation in ArI2 photodissociation dynamics

Bruno Lepetit, Octavio Roncero, Alexei A. Buchachenko, and Nadine Halberstadt

Citation: J. Chem. Phys. **116**, 8367 (2002); doi: 10.1063/1.1471907
View online: http://dx.doi.org/10.1063/1.1471907
View Table of Contents: http://jcp.aip.org/resource/1/JCPSA6/v116/i19
Published by the American Institute of Physics.

Additional information on J. Chem. Phys.

Journal Homepage: http://jcp.aip.org/
Journal Information: http://jcp.aip.org/about/about_the_journal
Top downloads: http://jcp.aip.org/features/most_downloaded
Information for Authors: http://jcp.aip.org/authors

ADVERTISEMENT

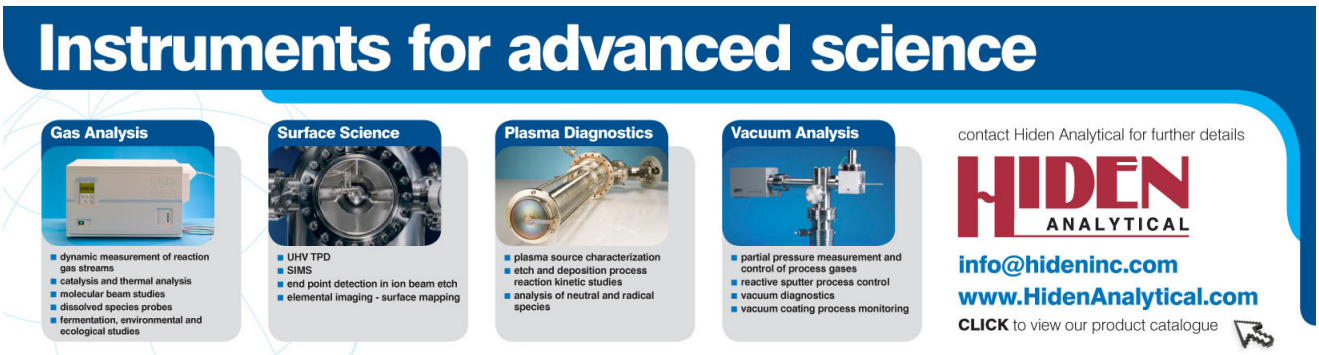

Downloaded 14 Mar 2013 to 161.111.22.69. Redistribution subject to AIP license or copyright; see http://jcp.aip.org/about/rights_and_permissions

Electronic and vibrational predissociation in ArI_2 photodissociation dynamics

Bruno Lepetit
LCAR-IRSAMC, Université Paul Sabatier et CNRS, UMR5589, F-31062 Toulouse Cedex, France

Octavio Roncero
Instituto de Matemáticas y Física Fundamental, C.S.I.C., Serrano 123, 28006 Madrid, Spain

Alexei A. Buchachenko
Laboratory of Molecular Structure and Quantum Mechanics, Department of Chemistry, Moscow State University, 119899 Moscow, Russia

Nadine Halberstadt
LPQ-IRSAMC, Université Paul Sabatier et CNRS, UMR5626, F-31062 Toulouse Cedex, France

(Received 2 January 2002; accepted 1 March 2002)

Quantum dynamical calculations on the photodissociation process: $ArI_2(X)+h\nu \rightarrow Ar+I_2(B)$ or Ar+I+I have been performed using diatomics-in-molecule semiempirical potential energy surfaces in the spectral region of the $I_2(B,v=15-25) \leftarrow I_2(X,v=0)$ transition. The B state responsible for vibrational predissociation producing $Ar+I_2(B)$ is coupled to four dissociative states inducing electronic predissociation to $Ar+I(^2P_{3/2})+I(^2P_{3/2})$. These dissociative states correlate to the $a(1g)$, $a'(0g^+)$, $B''(1u)$, $1(2g)$ electronic states of I_2. Both linear and perpendicular initial $ArI_2(X)$ isomers are considered. For the linear isomer, only the a' state has non-negligible effect on photodissociation dynamics, although total photon absorption cross sections are not significantly modified when coupling to a' is taken into account, partial cross sections corresponding to vibrational predissociation are smaller. For the perpendicular isomer, resonance decay rates are increased, mainly by the coupling to $a'(0g^+)$, $1(2g)$, and $a(1g)$ states. Decay rates oscillate as a function of the vibrational excitation of $I_2(B)$ but the main source of oscillation is the intramolecular vibrational energy redistribution which occurs in vibrational predissociation, rather than Franck–Condon oscillations in electronic predissociation. © *2002 American Institute of Physics.*
[DOI: 10.1063/1.1471907]

I. INTRODUCTION

The $Ar-I_2$ complex has been extensively studied in the excitation region of the bound levels of the excited $I_2(B)$ state, both experimentally and theoretically (for a recent review, see Ref. 1). These studies have provided a wealth of crucial information, not only on the structure of the complexes but also on the dynamics of vibrational and electronic predissociation.[2–11] The fluorescence excitation spectrum shows broadened features which are attributed to quasibound levels associated with $Ar-I_2(B,v')$, where v' refers to the vibrational excitation of the I_2 fragment. These resonances decay by two competing intramolecular relaxation processes:[8,12,13] vibrational predissociation (VP),

$$Ar-I_2(B,v') \overset{VP}{\rightarrow} Ar+I_2(B,v \leqslant v') \tag{1}$$

and complex-induced electronic predissociation (EP),

$$Ar-I_2(B,v') \overset{EP}{\rightarrow} Ar+I(^2P_{3/2})+I(^2P_{3/2}). \tag{2}$$

Since channel (1) produces electronically excited I_2 fragments which can fluoresce while channel (2) is dark, measurements of the I_2 fluorescence quantum yield in conjunction with $Ar-I_2$ absorption spectra provide the relative importance of vibrational predissociation (VP) as compared to the sum of electronic (EP) and vibrational predissociation. The vibrational predissociation efficiency (VPE) measured by Burke and Klemperer[8] presents oscillations as a function of the vibrational state from $v'=15$ to 26. These oscillations were attributed to EP, while the VP rate was assumed to vary monotonically with the initial population. Based on this model, the oscillations were reproduced by a simple golden rule treatment of the EP to a single dissociative electronic state yielding I+I+Ar products[14–16] as well as with a molecular dynamics method including quantum transitions.[17]

In the $v'=15-26$ band, VP takes place by the transfer of three vibrational quanta and is mediated by intramolecular vibrational redistribution (IVR).[2–5] Therefore, the monotonous increase of the VP rate with vibrational excitation assumed by Burke and Klemperer[8] can only be explained assuming the IVR statistical limit. However, quantum calculations neglecting EP showed that IVR occurs in the sparse limit; only a few zero-order quasibound states participate in the IVR,[18–23] and the VP rate presents strong oscillations with the initial vibrational excitation. One way to investigate further this contradiction on the role of IVR is to perform dynamical calculations on accurate electronic potential energy surfaces where vibrational predissociation is allowed to compete with electronic predissociation. EP could broaden linewidth of the intermediate levels in IVR, and thus

 © 2002 American Institute of Physics

Downloaded 14 Mar 2013 to 161.111.22.69. Redistribution subject to AIP license or copyright; see http://jcp.aip.org/about/rights_and_permissions

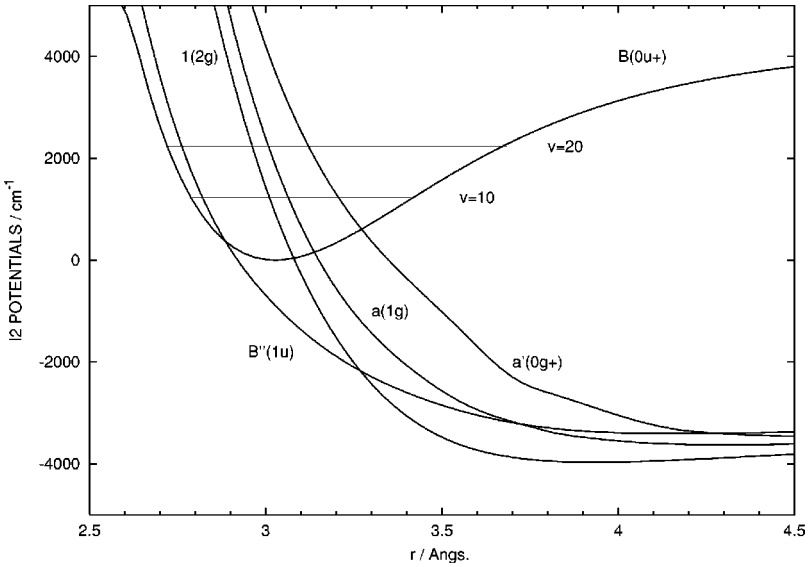

FIG. 1. I_2 potential energy curves as a function of the I–I distance. The four $B''(1u)$, $1(2g)$, $a(1g)$, and $a'(0g^+)$ curves cross the $B(0u^+)$ one. Couplings are induced between these states by the approach of the Ar atom. Distances are in angstroms, energies are in wave numbers, the zero is the minimum of the B potential. The $v=10$ and 20 vibrational levels are also shown.

make the system behave as in statistical IVR. In a molecular dynamics study with quantum transitions,[17] it was shown that first order rate equations were not adequate to describe the time dependent signals. This was attributed to the dependence of the EP rates on the vibrational quantum number of the intermediate state in the IVR process.

Six potential energy curves correlating to the ground $I(^2P_{3/2})+I(^2P_{3/2})$ cross the B state which correlates to the excited $I(^2P_{3/2})+I(^2P_{1/2})$.[24] Ar atom can only induce nonzero couplings from $B(0u^+)$ to 4 of these 6 states,[25–27] $B''(1u)$, $1(2g)$, $a(1g)$, $a'(0g^+)$ (see Fig. 1). In the strictly T-shape geometry, only coupling to the $a(1g)$ state survives. It is therefore tempting to assume that the $a(1g)$ state is the one responsible for EP.[14–16] The fact that oscillations of the EP rates as of function of the vibrational quantum number of the initially excited state are similar to those observed in the electric induced quenching of the B state of the isolated I_2 (Refs. 28 and 29) leads to the same conclusion. However, the complex initially excited to resonant states undergoes large amplitude vibrations and explores non-T-shape geometries where couplings from B to all 4 dissociative states are nonzero. This suggests that the other three dissociative states may also play a significant role in the EP process. Quasiclassical simulations on semiempirical DIM potential energy surfaces[27] indeed indicated that all 4 dissociative states contribute with comparable weights to electronic predissociation. This contradiction between different theoretical analyses also calls for new investigations on the role of the different electronic dissociative states in EP.

In this work, we study the competition of vibrational and electronic predissociation using fully quantum mechanical dynamical calculations with the $B(0u^+)$ state coupled to the 4 dissociative $B''(1u)$, $1(2g)$, $a(1g)$, $a'(0g^+)$ electronic states. We use diatomics-in-molecule (DIM) electronic potential energy surfaces and couplings[25,26] recently improved in Ref. 30. We analyze which of these electronic states have significant effects on the dynamics of the system for both linear and T-shape initial states. For the T-shape initial isomer, we study how IVR is effected by the occurrence of the electronic predissociation process. The present work is organized as follows. In Sec. II, we briefly recall the basic equations used in our model and give some computational details. We describe in Sec. III the electronic potential energy surfaces and couplings used in our work. We discuss in Sec. IV the absorption cross sections and resonant state lifetimes which result from the present calculations and confront them with available theoretical and experimental data.

II. METHOD

In the framework of the first order perturbation theory for electric dipole transitions, the cross section for photon excitation from an initial bound state $|\Psi_i\rangle$ to a final continuum state $|\Psi_{fE}\rangle$, is defined by[31]

$$\sigma_{fE\leftarrow i}\propto|\langle\Psi_{fE}|\mathbf{d}\cdot\mathbf{e}|\Psi_i\rangle|^2, \tag{3}$$

where $\mathbf{d}$ is the transition dipole moment and $\mathbf{e}$ is the polarization vector of the incident photon. We use in the present study the time dependent formalism; the cross section is then obtained as the Fourier transform of the auto correlation function, for a wave packet whose initial condition corresponds to the projection of $\mathbf{d}\cdot\mathbf{e}|\Psi_i\rangle$ on the B electronic state, and whose time evolution is governed by the Hamiltonian associated to the subspace spanned by the 5 coupled $B(0g^+)$, $B''(1u)$, $1(2g)$, $a(1g)$, $a'(0g^+)$ electronic states. This Hamiltonian is parametrized with Jacobi coordinates $(\mathbf{R},\mathbf{r})$, $\mathbf{R}$ being the vector joining the I_2 center-of-mass to the Ar atom and $\mathbf{r}$ the I_2 internuclear vector,

$$H=-\frac{\hbar^2}{2\mu_{\mathrm{Ar,I_2}}}\frac{\partial^2}{\partial R^2}+\frac{\mathbf{l}^2}{2\mu_{\mathrm{Ar,I_2}}R^2}-\frac{\hbar^2}{2\mu_{\mathrm{I_2}}}\frac{\partial^2}{\partial r^2}+\frac{\mathbf{n^2}}{2\mu_{\mathrm{I_2}}r^2}+H_{\mathrm{el}}(\mathbf{q_e};\mathbf{R},\mathbf{r}), \tag{4}$$

where $\mu_{\mathrm{Ar,I_2}}$ and $\mu_{\mathrm{I_2}}$ are reduced masses, $\mathbf{l}$ and $\mathbf{n}$ are angular momenta associated with $\mathbf{R}$ and $\mathbf{r}$, $H_{\mathrm{el}}(\mathbf{q_e};\mathbf{R},\mathbf{r})$ is the electronic Hamiltonian, and $\mathbf{q_e}$ are electronic coordinates. Note

Downloaded 14 Mar 2013 to 161.111.22.69. Redistribution subject to AIP license or copyright; see http://jcp.aip.org/about/rights_and_permissions

that the diatomic fragment may have an electronic angular momentum $\mathbf{j_e}$ so that its total angular momentum $\mathbf{j}$ is given by $\mathbf{j}=\mathbf{n}+\mathbf{j_e}$. The total angular momentum of the triatomic is $\mathbf{J}=\mathbf{l}+\mathbf{j}$.

In the spaced-fixed frame, $\mathbf{R}$ has spherical polar coordinates (θ_R,φ_R). In the frame defined by the Euler angles $(\varphi_R,\theta_R,0)$, the spherical polar angles of $\mathbf{r}$ are (θ_r,φ_r). We define a "triatomic" body frame such that the z-axis is $\mathbf{R}$ and the y-axis is parallel to $\mathbf{R}\times\mathbf{r}$. It is defined by the Euler angles $(\varphi_R,\theta_R,\varphi_r)$. We also use for the electronic wave function a "diatomic" body frame deduced from the triatomic one by a rotation of θ_r around the y-axis; its z-axis is $\mathbf{r}$ and its y-axis $\mathbf{R}\times\mathbf{r}$.

For a given total angular momentum J and projection M on the space-fixed axis, the total wave function Ψ^{JM} is expanded on a diabatic electronic basis $\phi_e^{\omega i\sigma}$ and Wigner rotation matrices $D^{J*}_{M\Omega}$ as

$$\Psi^{JM}(\mathbf{q_e},\mathbf{R},\mathbf{r})=\sum_{\Omega\omega i} D^{J*}_{M\Omega}(\varphi_R,\theta_R,\varphi_r) \times\Psi^{JM}_{\Omega\omega i}(R,r,\theta_r)\phi_e^{\omega i\sigma}(\mathbf{q_e}). \quad (5)$$

Here, Ω is the projection of the total angular momentum on the triatomic body frame axis. Electronic states are defined in the diatomic body frame and are labeled by the quantum numbers of the isolated diatomic; ω, the (signed) projection on the diatomic body frame z-axis of the total electronic angular momentum $\mathbf{j_e}$; $i=\pm1$, the effect of inversion of electronic coordinates in the diatomic body frame on the electronic wave functions; $\sigma=\pm1$, such that the effect of the symmetry through the triatomic molecular plane is $\sigma_v(xz)\phi_e^{\omega i\sigma}=\sigma\phi_e^{-\omega i\sigma}$. Definition of σ is unambiguous for $\omega=0$ states, however for $\omega\neq0$, it is necessary to fix (arbitrarily) the relative sign of $\phi_e^{-\omega i\sigma}$ with respect to $\phi_e^{\omega i\sigma}$ to obtain the value of σ. The components $\Psi^{JM}_{\Omega\omega i}(R,r,\theta)$ can be expanded in a basis of reduced Wigner rotation matrices associated with $\mathbf{j}=\mathbf{n}+\mathbf{j_e}$,

$$\Psi^{JM}_{\Omega\omega i}(R,r,\theta_r)=\sum_j \Psi^{JM}_{\Omega\omega ij}(R,r)d^j_{\Omega\omega}(\theta_r). \quad (6)$$

The wave function $\Psi^{JM}(\mathbf{q_e},\mathbf{R},\mathbf{r})$ is symmetrized ($\epsilon_\Pi=1$) or antisymmetrized ($\epsilon_\Pi=-1$) with respect to parity operation Π (defined as the inversion of all electronic and nuclear coordinates in the space-fixed frame) and permutation P ($\epsilon_P=\pm1$) of the 2 identical iodine atoms. The small Coriolis couplings induced by the rotation of the diatomic between different electronic states are neglected here.

We consider the following the transition: $ArI_2(X,J=1,\epsilon_\Pi=-1,\epsilon_P=-1)\rightarrow ArI_2(B,J=0,\epsilon_\Pi=1,\epsilon_P=-1)$. The initial vibrational state can be the ground state on the X DIM potential either for the T-shape or linear isomer. For the wave packet excited to the B state, 2 situations are considered; one where only VP is taken into account, only the B electronic state is included in the calculation; one where the B state is coupled to the other dissociative states. In practice, only the $a'(0g^+)$ is included for the linear initial isomer (see Sec. IV), but the four $B''(1u)$, $1(2g)$, $a(1g)$, $a'(0g^+)$ are included for the dynamics from the T-shape isomer. For simplicity reasons, a similar representation is used to represent the initial ground state and the time dependent wave packet; it consists of a 200×128 grid in the intervals $[5,25]\times[4.5,9]$ (in atomic units) for R and r, respectively, and of a basis of reduced Wigner rotation matrices [see Eq. (6)] with $j_{\max}=46$ for θ_r. In order to avoid too much energy spreading, the initial wave packet in the B state is projected on a reduced vibrational basis of the B electronic state, with $12\leqslant v'\leqslant28$. The wave function is propagated up to a maximum time of 10 ps for the linear isomer. For the T-shape isomer, the maximum time is 300 ps when the B state only is included, 120 ps when all 5 coupled electronic states are considered. For the T-shape isomer, the auto correlation function is still not zero at these final times. The auto correlation is thus damped by an artificial exponential factor $e^{-\overline{\Gamma}t/(2\hbar)}$ and then Fourier transformed. The spectrum results from the superposition of many lines, each individually broadened by the damping width $\overline{\Gamma}$. Predissociation rates are obtained by fitting these lines to Lorentzian shapes. The artificial broadening $\overline{\Gamma}$ must be subtracted from the results of these fits to yield physical widths and predissociation rates. The artificial broadening has been chosen as $\overline{\Gamma}=0.110\ \mathrm{cm}^{-1}$ for the calculation where the B state is coupled to the other ones and $\overline{\Gamma}=0.044\ \mathrm{cm}^{-1}$ for the calculation, where VP only is taken into account.

III. POTENTIAL ENERGY SURFACES AND COUPLINGS

All electronic structure parameters for dynamical calculations, namely, the potential energy surfaces of $X(0_g^+)$, $B(0_u^+)$, $B''(1_u)$, $1(2_g)$, $a(1_g)$, and $a'(0_g^+)$ electronic states and diabatic coupling matrix elements between $B(0_u^+)$ and $B''(1_u)$, $1(2_g)$, $a(1_g)$, $a'(0_g^+)$ states are evaluated using the consistent approach, first-order diatomics-in-molecule perturbation theory.[30] In brief, the zero-order adiabatic relativistic electronic wave functions are obtained by solving numerically inverse atoms-in-molecule problem for the valence states of isolated I_2 molecule at each internuclear distance r.[32] This procedure determines the wave function expansion coefficients over the Hund case (a) molecular functions. The latter are then expanded as the symmetrized products of atomic iodine functions and used to evaluate the matrix elements of the perturbation operator describing the interaction of I_2 and Ar fragments analytically in terms of interaction potentials of the Ar–I pair in $^2\Sigma^+$, $^2\Pi$ states, using the formulas presented in Ref. 33. Transformation of perturbation operator matrix to the basis of zero-order wave functions provides the final results; the diagonal elements give the interaction potential energy surfaces, while the nondiagonal ones represent diabatic coupling matrix elements.

The full description of this procedure will be given in a forthcoming publication, whereas its implementation to the $X(0_g^+)$ state of ArI_2 is described in Ref. 30. The inverse atoms-in-molecule problem for the valence states of I_2 is solved for the input set of relativistic potential energy curves composed from *ab initio* data by Teichteil and Pélissier[24] and available spectroscopic information (set TP2 in Refs. 30 and 32). The Ar–I potentials are taken from Ref. 34. In the dynamical calculations, spectroscopic potential energy curves are used for I_2 states, $X(0_g^+)$,[35] $B(0_u^+)$,[36] $B''(1_u)$,[29]

Downloaded 14 Mar 2013 to 161.111.22.69. Redistribution subject to AIP license or copyright; see http://jcp.aip.org/about/rights_and_permissions

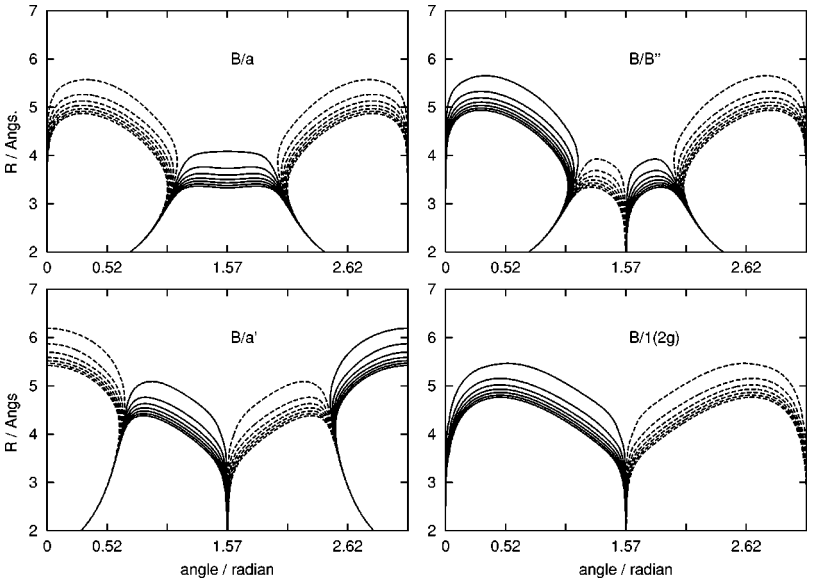

FIG. 2. Couplings between I_2 electronic states induced by the presence of the Ar atom, as a function of the bending angle θ_r and of the Ar–I_2 distance R in angstrom. The I_2 distance r corresponds to the $I_2(B)$ equilibrium distance $r=3$ Å. Contour values are -39, -33, $-27\ldots,-3$, $3,\ldots,27$, 33, 39 cm^{-1}, dashed lines corresponding to negative values.

$a(1_g)$,[29,37] and $a'(0_g^+)$,[38,39] while the $1(2_g)$ state is represented by an *ab initio* curve.[24] These potential energy curves are shown in Fig. 1. The code for generating all potential energy surfaces and couplings is available from the authors upon request. (Preferentially to A. A. Buchachenko at alexei@classic.chem.msu.su.)

Although the present approach is a refinement to the intermolecular DIM PT1 model which utilizes the asymptotic approximation for I_2 wave functions,[25,26] it inherits many features of the former. In particular, although the expressions for the coupling matrix elements become more complicated, they exhibit the same symmetry and selection rules as the simple expressions derived in Ref. 27 and used to study EP of ArI_2 within the quasiclassical model. In addition, the couplings between the B state and the $2(0_u^-)$ and (3_u) states, whose potential curves also cross the curve of the B state, vanish within both models. It should be noted also that the present calculations are completely consistent with our previous study of the ArI_2 VP (Ref. 23) because the potential energy surfaces for X and B states are the same.

The accuracy of X and B potential energy surfaces obtained with the DIM PT1 approach can be tested by comparison with the experimental dissociation energies of the van der Waals complex. For the T-shape isomer in the X state, we use as a reference the well established experimental value $D_0=237$ cm^{-1} (Refs. 3 and 11) instead of the more recent value 142 cm^{-1} (Ref. 9) which is subject to discussions. The present DIM value $D_0^{\mathrm{DIM}}=209$ cm^{-1} is in acceptable agreement with this experimental reference. For the B state, the agreement is even better; we get $D_0^{\mathrm{DIM}}=222$ cm^{-1}, compared to the equally well established experimental value 224 cm^{-1}. For the linear isomer in the X state, we obtain $D_0^{\mathrm{DIM}}=166$ cm^{-1}, to be compared to the recent experimental value,[9] 172 cm^{-1}.

Figure 2 shows the couplings between the B state and the four dissociating states for a fixed I–I distance $r_e=3$ Å. This coupling increases like $V_{\Pi}^{\mathrm{ArI}}-V_{\Sigma}^{\mathrm{ArI}}$ as Ar approaches the I_2 molecule. Nodal lines appear as a function of θ_r. Some are requested from symmetry considerations; the only nonzero couplings are $B(0u^+)-a'(0g^+)$ and $B(0u^+)-a(1g)$ for linear and T-shape geometries, respectively. An additional nodal line appears near $\theta_r=\pi/6$ for the a' states, and near $\theta_r=\pi/3$ for the a and B'' states. When one deviates from T-shape geometry (for R near to $R_e=3.8$ Å—the equilibrium distance in the B state), coupling increases quickly for the $a'(0g^+)$ and $1(2g)$ states, but remains small for $a(1g)$ and $B''(1u)$.

One can expect electronic predissociation for the linear isomer to be dominated by the $a'(0g^+)$ state, which is by far the most strongly coupled in linear and near linear geometries to the B state. For the T-shape isomer, the $a(1g)$ state is the only one with nonzero coupling to the B state in exact perpendicular geometries. However, this coupling remains small in near perpendicular geometries. On the other hand, the $1(2g)$ and $a'(0g^+)$ have zero couplings in perpendicular geometries, but the couplings increase quickly as one moves away from exact perpendicular geometries. $B''(1u)$ is weakly coupled for all perpendicular and near perpendicular geometries to the B state. For this reason, one can expect the $B''(1u)$ state to produce little electronic predissociation, but it is not clear which of the three $a(1g)$, $a'(0g^+)$ or $1(2g)$ states is going to be dominant. We will discuss these points further in Sec. IV B.

IV. RESULTS

A. Linear isomer dynamics

Figure 3 shows the population of the different dissociative electronic states as a function of time when the initial state is the linear isomer. Only short times are considered. One observes a sharp increase of the population near 30–100 fs, which then remains constant for longer times. The $a'(0g^+)$ state is by far the most populated; its population is two or three orders of magnitude larger than the one of the other three states. This results directly from the behavior of the electronic potentials for linear and near linear geometries, the $B-a'(0g^+)$ electronic coupling being the only one to be nonzero for linear geometries and larger than the others for

Downloaded 14 Mar 2013 to 161.111.22.69. Redistribution subject to AIP license or copyright; see http://jcp.aip.org/about/rights_and_permissions

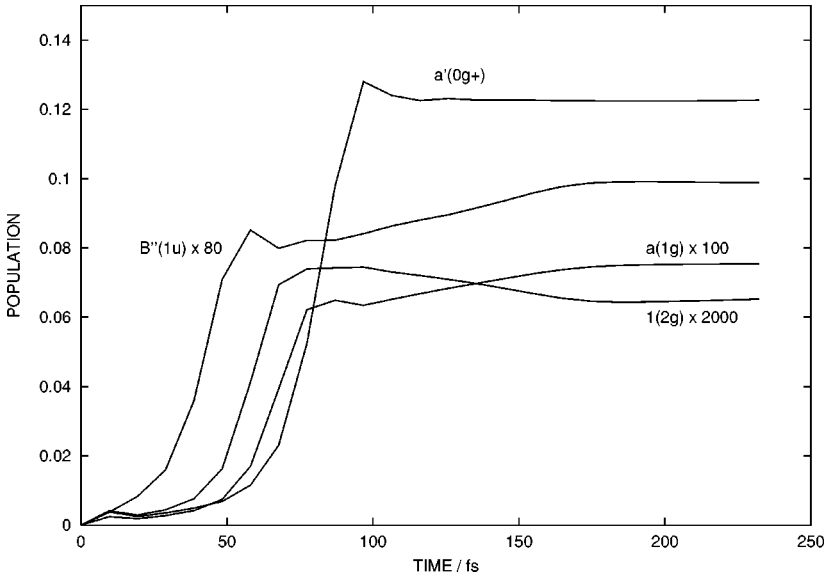

FIG. 3. Population of the different electronic states as a function of time (in femtoseconds). The initial wave packet corresponds to the linear isomer. Populations for the $B''(1u)$, $a(1g)$ and $1(2g)$ have been multiplied by 80, 100, and 2000, respectively.

near linear configurations. Therefore, we use in the following the single dissociative $a'(0g^+)$ state in the calculation of the photodissociation cross sections.

The time at which the increase of the a' population takes place can be correlated to the wave packet dynamics on the B potential. Vertical transition from the initial X state leads the wave packet to the repulsive part of the potential, especially in r and R. Indeed, equilibrium distances for the X state ($r_e^X = 2.7$ Å and $R_e^X = 5.2$ Å) are smaller than those for the B state ($r_e^B = 3$ Å and $R_e^B = 5.5$ Å). The early times dynamics of the wave packet center is shown in Fig. 4. It consists of an increase of both $\langle r \rangle$ and $\langle R \rangle$ (averages of the distances are defined with respect to the evolving wave packet). The increase in $\langle r \rangle$ is much larger than the one in $\langle R \rangle$, due to large differences in potential slopes. The wave packet center reaches the $B-a'$ crossing line and later the I_2 outer turning point. Then, it starts to oscillate in $\langle r \rangle$, whereas $\langle R \rangle$ starts to increase faster, thus crossing the $B-a'$ crossing line at increasingly larger R values. The sharp increase of the a' population occurs when the wave packet encounters the $B-a'$ crossing line for the first time. Subsequent crossings will not induce significant transitions; indeed, they occur at sufficiently larger R such that the electronic coupling has reduced significantly.

A crude estimate of the population of the $a'(0g+)$ can be obtained from a simple Landau–Zener formula[40] applied to the r degree of freedom, the two other degrees of freedom being frozen $R = R_e^X = 5.2$ Å, $\theta_r = 0$. For a velocity corresponding to the average energy of the wave packet, we obtain a Landau–Zener transition probability of 0.11, in very good agreement with the quantum result 0.12.

Figure 5 shows the total photodissociation (including both EP and VP) cross section as a function of excitation energy. This spectrum is almost identical to the one (not shown) which is obtained when coupling to the dissociative states are neglected (see Ref. 23, Fig. 4). The spectrum results from the superposition of a continuous background and peaks due to linear quasibound states. The continuous back-

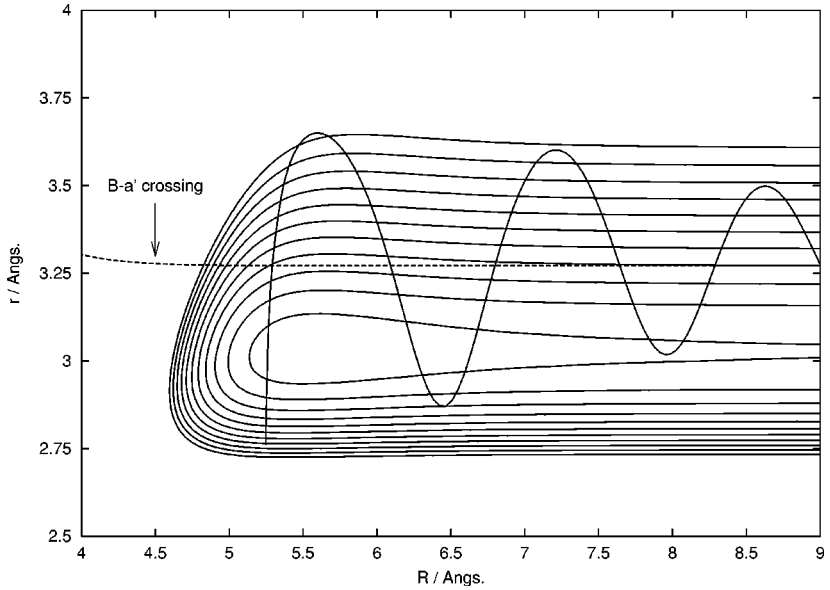

FIG. 4. Wave packet center trajectory on the B potential energy surface. The initial condition corresponds to the linear isomer. Also shown is the $B-a'(0g^+)$ crossing line. The contour values on the B potential are 0, 200, . . . , 2000 cm^{-1}.

Downloaded 14 Mar 2013 to 161.111.22.69. Redistribution subject to AIP license or copyright; see http://jcp.aip.org/about/rights_and_permissions

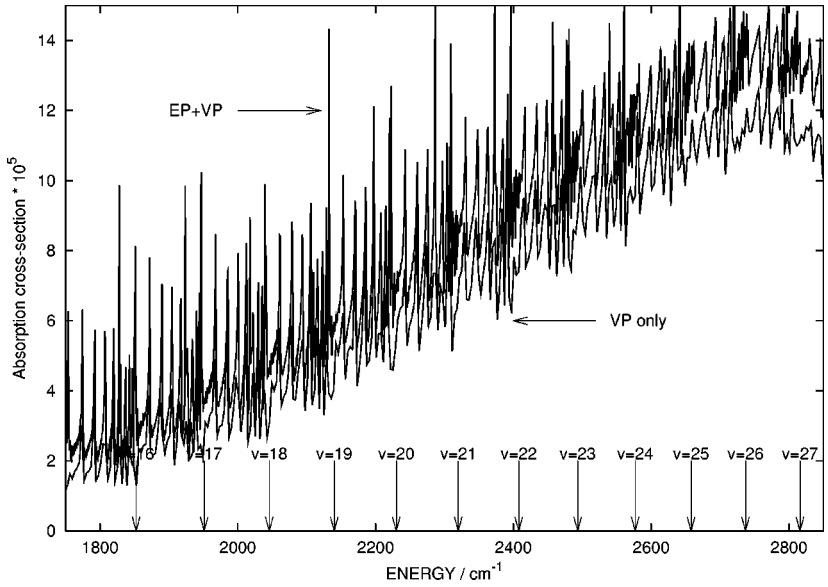

FIG. 5. Photon absorption cross sections as a function of excitation energy (in wave numbers, zero: minimum of the B potential at infinite $Ar–I_2$ distance). Cross sections are normalized such that the integral over energy is 1. EP+VP: full calculation, where the $B(0u^+)$ potential energy surface is coupled to the $a'(0g^+)$. VP: only the $B(0u^+)$ state is included in the calculation, EP cannot take place. $I_2(B,v)$ vibrational thresholds are also indicated.

ground results mainly from direct absorption to the continua $Ar+I_2(v')$, because as we already noted, a vertical transition from the initial state $Ar\cdots I_2(X)$ falls into the repulsive part of the $Ar\cdots I_2(B)$ potential. Peaks are due to quasibound states which can be assigned approximate quantum numbers (v,n) for the stretching modes in r (I_2 vibration) and R (van der Waals stretching). More on the interpretation of the spectrum can be found in Ref. 23. In particular, the bending quantum number is left undefined. Indeed, a single peak results from the contribution of several closely spaced bound states with different, but always small, bending excitations. Also shown in Fig. 5 is the partial cross section associated with the vibrational predissociation, in the presence of the competing electronic predissociation process. This partial spectrum is obtained by half Fourier transform of the time dependence of the coefficients of the wave function on the I_2 rovibrational basis at fixed $R(=20$ a.u.) (see Ref. 41). It has a lower resolution in energy than the total spectrum. It is clear that the main effect of EP is to reduce I_2 product state populations by roughly 10%. The other main features of the spectrum, in particular resonance positions and widths, are not significantly modified. This result is consistent with the early time analysis of Fig. 3; slightly more than 10% of the initial population is lost in the EP channel $Ar+I_2(a')$ at early time and cannot contribute to VP. However, subsequent time dynamics is not significantly effected by the EP channel, leaving resonances almost unchanged.

B. T-shape isomer dynamics

Figure 6 shows the population of the different dissociative electronic states as a function of time when the initial state is the T-shape isomer. Each population curve can be fitted to an exponential function depending on the population at large times p_∞ and the total decay rate k of the system: $\mathrm{pop}(t)=p_\infty(1-e^{-kt})$. Fits give a decay rate k of 30 ns^{-1} and relative populations p_∞ of 0.01, 0.05, 0.08, and 0.12 for the $B''(1u)$, $a(1g)$, $1(2g)$, and $a'(0g^+)$ states, respec-

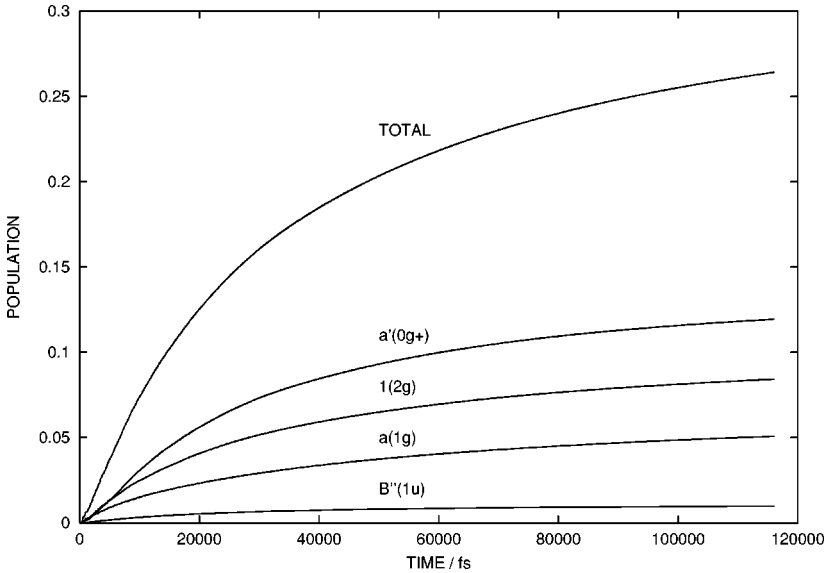

FIG. 6. Population of the different electronic states as a function of time (in femtoseconds). The initial wave packet corresponds to the perpendicular isomer in a coherent superposition of the different resonant states in the range $v'=12–28$ (see text). The curve labeled TOTAL is the sum of the 4 others.

Downloaded 14 Mar 2013 to 161.111.22.69. Redistribution subject to AIP license or copyright; see http://jcp.aip.org/about/rights_and_permissions

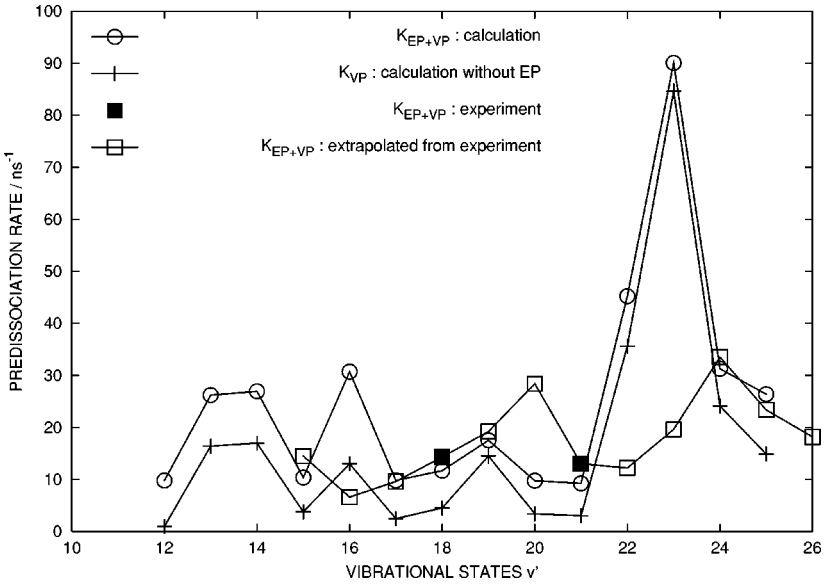

FIG. 7. Predissociation rates (in ns^{-1}) as a function of the resonant initial state vibrational excitation v'. The van der Waals bending–stretching mode is the ground one. Two calculation results are shown: k_{EP+VP}, full calculation, where the $B(0u^+)$ potential energy surface is coupled to the four dissociative states $B''(1u)$, $a(1g)$, $a'(0g^+)$, and $1(2g)$. k_{VP}: only the $B(0u^+)$ state is included in the calculation, EP cannot take place. Also shown is the experimental total rate from Ref. 8. This rate has been extrapolated from vibrational predissociation efficiencies VPE by assuming quasi-linear dependence of k_{VP} as a function of v'. Only the $v'=18$ and 21 rates result from direct measurements (Refs. 5 and 6) (see text).

tively. This indicates that, for the present potential energies and couplings, $a'(0g^+)$ state is the most important channel for EP, although it is uncoupled to the B state in the strictly T-shape geometry. As explained in Sec. III, this is due to the contribution of nonperpendicular geometries, which becomes important here because coupling increases quickly as a function of the bending angle away from the T-shape geometry. For similar reasons, the $1(2g)$ channel is also important, although slightly less. The $a(1g)$ channel, which can be coupled to the B state in strict T-shape geometry, has a population slightly less than half of the $a'(0g^+)$ and thus cannot be neglected. Only the $B''(1u)$ channel could be neglected in the calculation, contributing to EP one order of magnitude less. It was nevertheless kept, for the sake of completeness and accuracy.

The predissociation rates and branching ratios deduced from Fig. 6 are averaged ones, in the sense that they result from an initial B state which is a coherent superposition of all resonances which appear in the range $v'=12-28$ (see Sec. II B). Individual predissociation rates for each initial resonant state can be obtained from the Fourier transform of the auto correlation function and from fits of individual lines to Lorentzian shapes. The total (EP+VP) rates thus obtained are shown in Fig. 7 as a function of v'. For each v' the ground bending–stretching van der Waals mode has been selected. Indeed, most of the experimental results focus on this ground bending–stretching mode, for which absorption and fluorescence are the most intense.[5,6,8] The vibrational predissociation rate obtained from a quantum calculation with no EP (photodissociation on B state only, all electronic couplings being neglected) is also shown in Fig. 7. Total predissociation rates oscillate in the range 10–30 ns^{-1}, except around $v'=23$, where there is a sharp maximum which peaks to 90 ns^{-1}. In this case, the spectrum consists of several closely spaced Lorentzians with comparable weights, and the predissociation rates are obtained from weighted averages of the different linewidths.[20] The main source of oscillations in the total predissociation rate as a function of v' is the vibrational predissociation; the corresponding curve without EP oscillates similarly. These oscillations on the VP rates have been well characterized by previous quantum calculations as due to intramolecular vibrational redistribution (IVR) in the sparse limit. IVR results from quasidegeneracies between the initial excited state (bright state) $Ar\cdots I_2(v',n')$ and intermediate zero-order dark states with less I_2 vibrational excitation and more van der Waals bending and stretching energy $ArI_2(v'-1$ or $v'-2$, $n''\geqslant n')$. The vibrational coupling induced by the argon mixes these zero-order quasidegenerate states, which brings intensity to the dark states. These in turn provide coupling to the $Ar+I_2$ continuum. The small number of dark states in quasidegeneracy with a bright state is the fingerprint of the sparse limit of IVR in the present system. The main effect of EP is to increase the VP rates by 10 ns^{-1} on average. Its contribution is dependent on the initial vibrational excitation, but significantly less than VP, so that it is not the main contributor to the oscillations on the total rates.

Figure 7 also shows the experimental results from Refs. 5, 6, and 8. Predissociation rates have been measured by real time picosecond experiments for $v'=18$ and 21 only.[5,6] A good agreement between the direct real time experimental results and our estimates is obtained; experimental predissociation rates[5,6] are 14.3 and 13 ns^{-1} for $v'=18$ and 21, and the corresponding calculated rates are 11.7 and 9.2 ns^{-1}. Predissociation rates for other v' have been obtained in Ref. 8 by assuming a quasilinear dependence of the VP rates on v'. This amounts to assuming statistical limit IVR on VP. It is therefore not surprising that near $v'=23$, where IVR is strong according to our quantum results, serious discrepancies with these extrapolated results appear.

Although we have shown total rates only and have not yet fully converged VPE, we can define an approximate VPE by $\mathrm{VPE}=k_{VP}/k_{VP+EP}$. Here, k_{VP} is the rate obtained from a calculation with the single B state (EP being neglected), k_{VP+EP} is the total predissociation rate, including all dissociative states. This approximate VPE results from a first order kinetic scheme, where the VP rate in presence of EP is the same as the one without EP. This approximate VPE is

Downloaded 14 Mar 2013 to 161.111.22.69. Redistribution subject to AIP license or copyright; see http://jcp.aip.org/about/rights_and_permissions

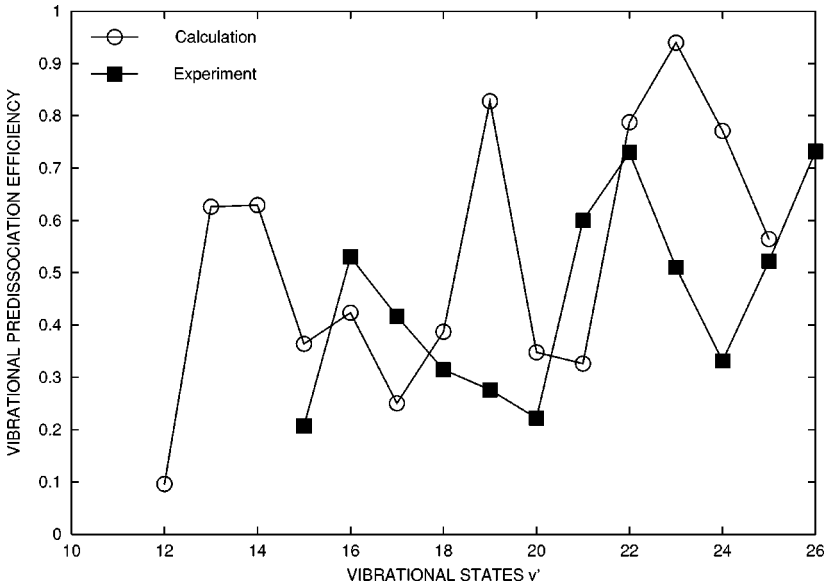

FIG. 8. Vibrational predissociation efficiency VPE as a function of vibrational excitation for the ground bending–stretching van der Waals mode. The results from the present calculation are compared to the experimental result from Ref. 8. The calculated VPE is obtained from the approximation, VPE$=k_{\mathrm{VP}}/k_{\mathrm{EP+VP}}$. k_{VP} is calculated by assuming no coupling to the dissociative states, EP cannot take place. $k_{\mathrm{EP+VP}}$ is the result of the calculation with the five coupled electronic states.

shown in Fig. 8, together with the experimental result. Theoretical and experimental oscillations as a function of v' occur with comparable amplitudes, but theoretical ones are shifted by a few vibrational quanta. The maxima in VPE correlate to the maxima in k_{VP} induced by IVR. The subtle balance between the weak vibrational and electronic couplings is thus well reproduced in our calculation. This indicates that IVR may well be the cause of the observed oscillations in VPE. However, IVR in the sparse limit results from accidental quasidegeneracies between resonant states with different vibrational and van der Waals excitation and is strongly dependent on details of the *B* potential.[18–20] It is therefore possible that slight modifications of the *B* potential may be enough to shift the maxima in the VP rate, producing calculated VPE closer to the measured ones.

Additional calculations on EP using a time dependent Golden Rule treatment (TDGR) were also performed following the method previously described in Refs. 15 and 16. In that previous work, a model potential was built such that the EP rate to the $a(1g)$ state presents oscillations which match the experimental ones. Two major ingredients were used. First, the $\mathrm{Ar}-\mathrm{I}_2(a(1g))$ van der Waals interaction was designed to present an attractive well so that it is I_2(a) which dissociates, leaving the wave packet in the van der Waals modes nearly unchanged during the full process (spectator model). It was found that if this was not the case the oscillations in the EP rate vanished. Second, the oscillations were attributed to the $a(1g)$ state and for that reason the strength of the $B-a(1g)$ coupling was fit to reproduce the experimental oscillations[8] within the TDGR treatment. Following similar arguments more recent molecular dynamics calculations also found similar oscillations.[17] Here, with the present DIM potential in which there is no adjustment of the parameters, the TDGR treatment gives physically similar results. In particular, we obtain the same kind of oscillations as a function of the initial vibrational excitation, demonstrating the adequacy of the spectator model. The main difference with the previous TDGR results concerns the amplitude of the oscillations, which previously was fit to reproduce the experimental oscillations, while here it is given by the electronic potentials and couplings with no possible adjustment. Therefore, for the $a(1g)$ state the oscillations are present, similarly to the previous cases, but are much less important than the experimental ones. Concerning the B'' state, the rate is much lower when using a TDGR treatment and presents less oscillations, as expected from a simple Franck–Condon model,[14] and the spectator model is no longer valid, since the wave packet in the van der Waals modes moves rapidly. For the other two dissociative $a'(0g)$ and $1(2g)$ states, there are also oscillations (the spectator model only works partially) but they do not match those of the $a(1g)$ state. Therefore, the total electronic rate, even at this simple TDGR level, presents less oscillations than the contribution of each electronic state. All these TDGR results are in agreement with the full calculations presented in this work and corroborate the fact that the main source of oscillations in the present system is IVR in the *B* electronic state.

Although obtained for zero total angular momentum, the present results should remain valid when global rotation of the complex is taken into account. In Ref. 22, it is shown that the nonstatistical sparse limit IVR mechanism is operative in ArI_2 vibrational predissociation for total angular momentum up to $J=24$. Although the density of dark states increases as a function of *J*, only a few of them play a role in the dissociation of a given bright state. In addition, the vibrational dependence of the VP rates on vibrational excitation v' was found to survive rotational averaging for a given van der Waals state.[21]

Whether sparse limit IVR is seen experimentally on this system is still a controversial issue. Burke and Klemperer[8] stated that IVR is in the statistical limit because fluorescence intensities have similar patterns as a function of v' for the three lowest bending excitation modes. However recent final rotational distributions[11] show structures which may be reminiscent of the stronger oscillations which appear in the computational results and which are clear evidences of sparse limit IVR in the theoretical models.[23] Therefore, new mea-

Downloaded 14 Mar 2013 to 161.111.22.69. Redistribution subject to AIP license or copyright; see http://jcp.aip.org/about/rights_and_permissions

surements of predissociation rates would be useful to elucidate the role of IVR in the predissociation process.

V. CONCLUSIONS

We have performed a quantum dynamical study of the $Ar\ldots I_2(B,v'=12-25)$ predissociation where both electronic and vibrational processes can take place. We used a set of 5 coupled DIM electronic potentials. For the linear initial isomer, we have shown that the only electronic state which has a non-negligible influence on the VP process is the $a'(0g^+)$. By contrast, for the *T*-shape isomer, the 3 channels $a'(0g^+)$, $1(2g)$, and $a(1g)$ can contribute significantly. Sparse limit IVR is the main contributor to oscillations in predissociation rates and VPE.

The present results remain to be further confirmed by new studies. In the short term, we plan to fully converge vibrational predissociation efficiencies. This would provide information on the effects of EP on rovibrational product state distributions. This will require a product state analysis and longer propagation times. Potential energy surfaces may also deserve further studies. Although currently we have no alternative to the DIM model and although DIM is able to reproduce experimental data on the transition frequencies and predissociation rates reasonably well, it would be extremely useful to check the model against other theoretical approaches, first of all high level *ab initio* ones. Finally, we also feel the lack of experimental results, whereas VPE have been measured for a wide range of v', total predissociation rates have been directly measured for only two v' values. Measuring these total predissociation rates for a large range of v' values would allow to assess definitely whether the origin of the oscillations is IVR in the VP process or Franck–Condon factors in the EP process.

ACKNOWLEDGMENTS

This work has been supported by DGICYT [Ministerio de Educación y Ciencia (MEC), Spain] under Grant No. PB95-0071, INTAS under Grant No. 97-31573, and the Spanish–French PICASSO Project No. HF1999-0132. A.A.B. also thanks MEC for sabbatical fellowship. An allocation of CPU time on the NEC SX-5 vector computer of the ''Institut du Developement et des Ressources Informatiques Scientifiques'' is gratefully acknowledged. We thank J. Alberto Beswick for many inspiring discussions.

[1] A. Rohrbacher, N. Halberstadt, and K. C. Janda, Annu. Rev. Phys. Chem. **51**, 405 (2000).
[2] G. Kubiak, P. S. H. Fitch, L. Wharton, and D. H. Levy, J. Chem. Phys. **68**, 4477 (1978).
[3] J. A. Blazy, B. M. DeKoven, T. D. Russell, and D. H. Levy, J. Chem. Phys. **72**, 2439 (1980).
[4] K. E. Johnson, W. Sharfin, and D. H. Levy, J. Chem. Phys. **74**, 163 (1981).
[5] J. J. Breen, D. M. Willberg, M. Gutmann, and A. H. Zewail, J. Chem. Phys. **93**, 9180 (1990).
[6] D. M. Willberg, M. Gutmann, J. J. Breen, and A. H. Zewail, J. Chem. Phys. **96**, 198 (1992).
[7] M. L. Burke and W. Klemperer, J. Chem. Phys. **98**, 1797 (1993).
[8] M. L. Burke and W. Klemperer, J. Chem. Phys. **98**, 6642 (1993).
[9] A. E. Stevens Miller, Ch. Chuang, H. C. Fu, K. F. Higgins, and W. Klemperer, J. Chem. Phys. **111**, 7844 (1999).
[10] A. Burroughs, T. Van Marter, and M. C. Heaven, J. Chem. Phys. **111**, 2478 (1999).
[11] A. Burroughs and M. C. Heaven, J. Chem. Phys. **114**, 7027 (2001).
[12] D. H. Levy, Adv. Chem. Phys. **47**, 323 (1981).
[13] J. A. Beswick and J. Jortner, Adv. Chem. Phys. **47**, 363 (1981).
[14] O. Roncero, N. Halberstadt, and J. A. Beswick, ''Caging and nonadiabatic electronic transitions in I_2–M complexes,'' in *Reaction Dynamics in Clusters and Condensed Phases*, edited by J. Jortner, R. D. Levine, and B. Pullmann (Kluwer Academic, Dordrecht, 1994), p. 73.
[15] O. Roncero, N. Halberstadt, and J. A. Beswick, Chem. Phys. Lett. **226**, 82 (1994).
[16] O. Roncero, N. Halberstadt, and J. A. Beswick, J. Chem. Phys. **104**, 7554 (1996).
[17] A. Bastida, J. Zúñiga, A. Requena, N. Halberstadt, and J. A. Beswick, Chem. Phys. **240**, 229 (1999).
[18] S. K. Gray, Chem. Phys. Lett. **197**, 86 (1992).
[19] S. K. Gray and O. Roncero, J. Phys. Chem. **99**, 2512 (1995).
[20] O. Roncero and S. K. Gray, J. Chem. Phys. **104**, 4999 (1996).
[21] E. M. Goldfield and S. K. Gray, Chem. Phys. Lett. **276**, 1 (1997).
[22] E. M. Goldfield and S. K. Gray, J. Chem. Soc., Faraday Trans. **93**, 909 (1997).
[23] O. Roncero, B. Lepetit, J. A. Beswick, and A. A. Buchachenko, J. Chem. Phys. **115**, 6961 (2001).
[24] C. Teichteil and M. Pélissier, Chem. Phys. **180**, 1 (1994).
[25] A. Buchachenko and N. F. Stepanov, J. Chem. Phys. **104**, 9913 (1996).
[26] A. Buchachenko and N. F. Stepanov, J. Chem. Phys. **106**, 4358 (1997).
[27] A. A. Buchachenko, Chem. Phys. Lett. **292**, 273 (1998).
[28] F. W. Dalby, C. D. P. Levy, and J. Vanderlinde, Chem. Phys. **85**, 23 (1984).
[29] J. Tellinghuisen, J. Chem. Phys. **82**, 4012 (1985).
[30] A. A. Buchachenko, O. Roncero, and N. F. Stepanov, Russ. J. Phys. Chem. **74**, S193 (2000).
[31] A. Schinke, *Photodissociation Dynamics* (Cambridge University Press, Cambridge, 1993).
[32] E. A. Pazyuk, A. V. Stolyarov, V. I. Pupyshev, N. F. Stepanov, S. Ya. Umanskii, and A. A. Buchachenko, Mol. Phys. **99**, 91 (2000).
[33] A. A. Buchachenko and N. F. Stepanov, Russ. J. Phys. Chem. **72**, 69 (1998).
[34] Y. Zhao, T. Yourshaw, G. Reiser, C. C. Arnold, and D. M. Neumark, J. Chem. Phys. **101**, 6538 (1994).
[35] F. Martin, R. Bacis, S. Churassy, and J. Vergés, J. Mol. Spectrosc. **116**, 71 (1986).
[36] S. Gerstenkorn and P. Luc, J. Phys. (Paris) **46**, 865 (1985).
[37] S. Churassy, F. Martin, R. Bacis, J. Vergés, and R. W. Field, J. Chem. Phys. **75**, 4863 (1981).
[38] F. Martin, S. Churassy, R. Bacis, R. W. Field, and J. Vergés, J. Chem. Phys. **79**, 3725 (1983).
[39] K. P. Lawley, M. A. MacDonald, R. J. Donovan, and A. Kvaran, Chem. Phys. **92**, 322 (1982).
[40] L. Landau and E. Lifchitz, *Quantum Mechanics*, Moscow ed. (1967).
[41] G. G. Balint-Kurti, R. N. Dixon, and C. C. Marston, J. Chem. Soc., Faraday Trans. **86**, 1741 (1990).

Downloaded 14 Mar 2013 to 161.111.22.69. Redistribution subject to AIP license or copyright; see http://jcp.aip.org/about/rights_and_permissions